Title

Radioprotection of the Brain White Matter by Mn(III) N-Butoxyethylpyridylporphyrin–Based Superoxide Dismutase Mimic MnTnBuOE-2-PyP5+

Journal

Molecular Cancer Therapeutics, 14(1)

ISSN

1535-7163

Authors

Weitzel, Douglas H
Tovmasyan, Artak
Ashcraft, Kathleen A
et al.

Publication Date

2015

DOI

10.1158/1535-7163.mct-14-0343

Peer reviewed

HHS Public Access

Author manuscript

Mol Cancer Ther. Author manuscript; available in PMC 2016 January 01.

Published in final edited form as:

Mol Cancer Ther. 2015 January ; 14(1): 70–79. doi:10.1158/1535-7163.MCT-14-0343.

Radioprotection of the Brain White Matter by Mn(III) *N*-Butoxyethylpyridylporphyrin-Based Superoxide Dismutase Mimic MnTnBuOE-2-PyP^{5+}

Douglas H. Weitzel[1], **Artak Tovmasyan**[1], **Kathleen A. Ashcraft**[1], **Zrinka Rajic**[1], **Tin Weitner**[1], **Chunlei Liu**[2], **Wei Li**[2], **Anne F. Buckley**[3,4,5], **Mark R. Prasad**[1], **Kenneth H. Young**[1], **Ramona M. Rodriguiz**[6], **William C. Wetsel**[6,7], **Katherine B. Peters**[8], **Ivan Spasojevic**[9], **James E. Herndon II**[10], **Ines Batinic-Haberle**[1], and **Mark W. Dewhirst**[1,4]

[1]Department of Radiation Oncology, Duke University Medical Center, Durham, North Carolina.

[2]Brain Imaging and Analysis Center, Duke University Medical Center, Durham, North Carolina.

[3]Department of Pathology, Duke University Medical Center, Durham, North Carolina.

[4]Preston Robert Tisch Brain Tumor Center, Duke University Medical Center, Durham, North Carolina.

[5]Animal Pathology Core, Duke University Medical Center, Durham, North Carolina.

[6]Department of Psychiatry and Behavioral Sciences, Duke University Medical Center, Durham, North Carolina.

Corresponding Author: Mark W. Dewhirst, Duke University Medical Center, Box 3455, Medical Sciences Research Building 1, Durham, NC 27710. Phone: 919-684-4180; Fax: 919-684-8718; dewhirst@radonc.duke.edu.
Current address for W. Li: Research Imaging Institute and Department of Ophthalmology, University of Texas Health Science Center at San Antonio, San Antonio, TX 78229.

Note: Supplementary data for this article are available at Molecular Cancer Therapeutics Online (http://mct.aacrjournals.org/).

Disclosure of Potential Conflicts of Interest

I. Spasojevic has ownership interest (including patents) and is a consultant/advisory board member for BioMimetix. I. Batinic-Haberle is consultant for BioMimetix, and has ownership interest (including patents) and is a consultant/advisory board member for BioMimetix JVLLC. M.W. Dewhirst reports receiving a commercial research grant from BioMimetix. No potential conflicts of interest were disclosed by the other authors.

Authors' Contributions

Conception and design: A. Tovmasyan. W.C. Wetsel, K.B. Peters, I. Batinic-Haberle, M.W. Dewhirst
Development of methodology: C. Liu, I. Spasojevic, I. Batinic-Haberle
Acquisition of data (provided animals, acquired and managed patients, provided facilities, etc.): D.H. Weitzel, A. Tovmasyan, K.A. Ashcraft, C. Liu, W. Li, M.R. Prasad, R.M. Rodriguiz. I. Spasojevic
Analysis and interpretation of data (e.g., statistical analysis, biostatistics, computational analysis): D.H. Weitzel, A. Tovmasyan, T. Weitner, C. Liu, A.F. Buckley, M.R. Prasad, K.H. Young, R.M. Rodriguiz, W.C. Wetsel, I. Spasojevic. J.E. Herndon H, I. Batinic-Haberle, M.W. Dewhirst
Writing, review, and/or revision of the manuscript: D.H. Weitzel, A. Tovmasyan, K.A. Ashcraft, C. Liu, A.F. Buckley. R.M. Rodriguiz, W.C. Wetsel, K.B. Peters, I. Spasojevic, J.E. Herndon H, I. Batinic-Haberle, M.W. Dewhirst
Administrative, technical, or material support (i.e., reporting or organizing data, constructing databases): D.H. Weitzel, K.H. Young
Study supervision: C. Liu, I. Batinic-Haberle, M.W. Dewhirst
Other [performed experiments (related to radiosensitization of Mn porphyrin) and drug development): Z. Rajic
Other (acquisition, organization of databases, analyses/interpretation, writing and review of results for those data pertaining to behavioral testing in the animals): R.M. Rodriguiz
Other (provided the radioprotector, optimized Mn porphyrin, MnTnBuOE-2-PyP, which was developed by the author and had a patent, and performed the radiosensitizing study on mice bearing tumors with it within this article): I. Batinic-Haberle

[7]Department of Neurobiology and Cell Biology, Duke University Medical Center, Durham, North Carolina.

[8]Medicine and Duke Cancer Institute, Duke University Medical Center, Durham, North Carolina.

[9]PK/PD BioAnalytical DCI Shared Resource, Duke University Medical Center, Durham, North Carolina.

[10]Biostatistics and Bioinformatics, Duke University Medical Center, Durham, North Carolina.

Abstract

Cranial irradiation is a standard therapy for primary and metastatic brain tumors. A major drawback of radiotherapy (RT), however, is long-term cognitive loss that affects quality of life. Radiation-induced oxidative stress in normal brain tissue is thought to contribute to cognitive decline. We evaluated the effectiveness of a novel mimic of superoxide dismutase enzyme (SOD), MnTnBuOE-2-PyP^{5+} (Mn(III) meso-tetrakis(*N*-n-butoxyethylpyridinium-2-yl)porphyrin), to provide long-term neuroprotection following 8 Gy of whole brain irradiation. Long-term RT damage can only be assessed by brain imaging and neurocognitive studies. C57BL/6J mice were treated with MnTnBuOE-2-PyP^{5+} before and after RT and evaluated three months later. At this time point, drug concentration in the brain was 25 nmol/L. Mice treated with MnTnBuOE-2-PyP^{5+}/RT exhibited MRI evidence for myelin preservation in the corpus callosum compared with saline/RT treatment. Corpus callosum histology demonstrated a significant loss of axons in the saline/RT group that was rescued in the MnTnBuOE-2-PyP^{5+}/RT group. In addition, the saline/RT groups exhibited deficits in motor proficiency as assessed by the rotorod test and running wheel tests. These deficits were ameliorated in groups treated with MnTnBuOE-2-PyP^{5+}/RT. Our data demonstrate that MnTnBuOE-2-PyP^{5+} is neuroprotective for oxidative stress damage caused by radiation exposure. In addition, glioblastoma cells were not protected by MnTnBuOE-2-PyP^{5+} combination with radiation *in vitro*. Likewise, the combination of MnTnBuOE-2-PyP^{5+} with radiation inhibited tumor growth more than RT alone in flank tumors. In summary, MnTnBuOE-2-PyP^{5+} has dual activity as a neuroprotector and a tumor radiosensitizer. Thus, it is an attractive candidate for adjuvant therapy with RT in future studies with patients with brain cancer.

Introduction

Radiation therapy (RT) is part of the standard of care for the treatment of brain tumors. However, RT can injure normal tissue, in part, through the generation of oxidative stress (1). Oxidative stress contributes to the deterioration of healthy brain tissue manifested by progressive loss of neurocognitive function. This affects function in adults, but it is especially troubling in children (2–4). Minimizing these RT effects on normal tissue would both greatly preserve brain function and improve the quality of life in these patients. The efficacy of RT is often limited by the extent of damage of normal tissue. Therefore, selectively reducing the oxidative damage of healthy brain tissue may allow the use of higher radiation doses to treat tumors.

Redox-active drugs have been successfully used *in vitro* and *in vivo* models of oxidative stress–related diseases (5). Flavonoid and organosulfur compounds have recently been shown to reduce RT-induced reactive oxygen species (ROS) and rescue the neurocognitive/neuromotor performance of cranially irradiated mice (6, 7). Our porphyrin-based series of SOD mimics catalytically react with a range of reactive species (e.g., superoxide, peroxynitrite, and carbonate radical) to restore the physiologic cellular redox environment (8, 9). These porphyrin compounds also protect normal tissues by attenuating the signaling of master transcription factors NF-κB and HIF1α, which govern inflammatory and hypoxia responses, respectively (8, 10, 11). Three lead compounds have been developed: Mn(III) *meso*-tetrakis (*N*-ethylpyridinium-2-yl)porphyrin (MnTE-2-PyP^{5+}), Mn(III)*meso*-tetrakis(*N*-n-hexylpyridinium-2-yl)porphyrin (MnTnHex-2-PyP^{5+}), and Mn(III)*meso*-tetrakis(*N*-n-butoxy*e*thylpyridinium-2-yl)porphyrin (MnTnBuOE-2-PyP^{5+}; Fig. 1A). MnTE-2-PyP^{5+} was the first compound developed. Because of its hydrophilicity, a 5,000-fold more lipophilic analogue was developed with lengthened hexyl alkylpyridyl chains, MnTnHex-2-PyP^{5+}. Its higher mitochondrial distribution and transfer across the blood–brain barrier(BBB) have been demonstrated (12, 13). Insertion of oxygen atoms into its hydrophobic chains resulted in the synthesis of MnTnBuOE-2-PyP^{5+}, which showed less toxicity than MnTnHex-2-PyP^{5+} while maintaining high lipophilicity and redox-related performance (14). Both MnTE-2-PyP^{5+} and MnTnHex-2-PyP^{5+} have protected normal rat lung from RT-induced oxidative stress (15, 16). In addition, Mn(III)tetrakis(*N*-methyl-2-pyridyl)porphyrin (MnTM-2-PyP^{5+}) protected mice from death following whole-body irradiation (17). The radioprotective effects of MnTnBuOE-2-PyP^{5+} on normal tissue have yet to be characterized.

Although general antioxidant therapies may protect normal tissues, a debate exists on their effectiveness toward tumor cells or attenuation of anticancer therapy efficacy (5). Tumor cells generally have increased superoxide and hydrogen peroxide production that promotes proliferation (18, 19). Our porphyrin compounds have been used both as anticancer agents in their own right and in combination with radiation and chemotherapy (20, 21). MnTnHex-2-PyP^{5+} treatment alone increased the survival of mice with intracranial tumors (pediatric medulloblastoma and glioblastoma multiforme; ref. 22) and decreased the tumor growth rate in a breast cancer model (11). In addition, MnTE-2-PyP^{5+} significantly enhanced radiation effects on breast and prostate tumor growth delay in mice (8, 21, 23). Because our porphyrin compounds have not shown protective effects toward tumor cells or tissues, they may serve a dual role with RT by negatively affecting tumors while simultaneously protecting normal tissues.

Herein, we demonstrate the radioprotective effects of MnTnBuOE-2-PyP^{5+} on normal brain tissue. In addition, we evaluated the tumor cell response to RT with or without MnTnBuOE-2-PyP^{5+} *in vitro* and *in vivo*. We demonstrate that MnTnBuOE-2-PyP^{5+} increases the antitumor effectiveness of RT in a glioblastoma xenograft model.

Materials and Methods

Mn porphyrin

MnTnBuOE-2-PyP^{5+} (Fig. 1A) prepared by GMP scale-up was used for this study (14).

Irradiation of neurocognition study group

One hundred C57B1/6J mice were divided equally into four treatment and control groups (Fig. 1B). MnTnBuOE-2-PyP^{5+} was prepared in sterile 0.9% saline and injected subcutaneously into mice randomly along the back. Animals were irradiated with 8 Gy delivered with parallel opposed beams using the X-RAD 225Cx irradiator (Precision X-Ray) with 225 kVp/13 mA settings. A 10 × 40 mm collimator was used to direct the beam only to the cranium, and placement of animals was confirmed by fluoroscopy. Control mice were anesthetized for similar durations as RT-treated mice. Animals were provided free access to food and water. During behavioral assessments, mice were maintained on a 14-hour light/10-hour dark cycle. All behavioral tests were conducted between 1,000 to 1,600 hours. All animal studies were performed in accordance with protocols approved by the Duke University Institutional Animal Care and Use Committee.

Neurocognitive and activity testing

Mice were behaviorally assessed for motor performance on the rotorod and for spontaneous activity in running wheels. Cognitive performance was evaluated in the Morris water maze, novel object recognition, and fear conditioning tests. One cohort of mice (10 mice/treatment condition) was examined on the rotorod (Med Associates, Inc.). On day 1, animals were tested (5 trials with 20 minutes intertribal interval) on the accelerating (4–40 rpm) rotorod over 5 minutes and on day 2 they were evaluated at a steady speed (28 rpm; refs. 24, 25). These same mice were examined one week later in a novel object recognition task for short-term (STM) and long-term memory (LTM; refs. 24–26). Finally, 5 mice from each treatment condition were placed individually into cages with running wheels (Coulbourn Instalments) to examine motor activity over a 24-hour period. Running wheel activity was monitored with Clock Lab data collection and analysis software (Actimetrics; ref. 27). A second cohort of mice was matched for age and sex across treatments (10 mice/treatment condition) and was tested in the Morris water maze over 12 days (24, 25). One week later, these mice were tested in contextual and cued fear conditioning (24). Briefly, mice were trained and tested over 2 days in mouse fear conditioning chambers (Med-Associates). For conditioning, mice were placed individually into the apparatus for 2 minutes, a 72-dB 12-kHz tone (conditioned stimulus, CS) was presented for 30 seconds, and the CS terminated simultaneously with a 2-second 0.4-mA scrambled foot-shock (unconditioned stimulus, UCS). The mouse remained in the chamber for 30 seconds and was removed to its home cage. Twenty-four hours later, mice were tested either in contextual or cued fear conditioning. For the former, one half of the mice were placed into the chamber in which they had been conditioned for 5 minutes in the absence of the CS and UCS. For the cued test, the remaining half of the animals was placed into a novel chamber for 2 minutes, subsequently the CS was presented for 3 minutes in the absence of the UCS. All behaviors were videotaped and scored with the Noldus Observer program (Noldus Information Technology) for freezing behaviors by trained observers blinded to the treatment conditions of the mice. Freezing was defined as the absence of all visible movement except that required for respiration (28, 29).

Tumor growth study

D-245 MG glioblastoma cells [kindly provided by the Preston Robert Tisch Brain Tumor Center (PRTBC) at Duke University, short tandem repeat (SIR) verification performed by PRTBC on July 15, 2004, and cells were used within 6 months of thaw (2011)] were inoculated subcutaneously in the right flank of mice (separate from the neurocognition study mice). Once tumors reached approximately 65 mm^3 (day 0), BALB/c nu/nu mice were randomly assigned to 4 groups with 8 mice per group: saline, saline/RT, MnP, and MnP/RT. Mice were injected subcutaneously with 1.6 mg/kg MnTnBuOE-2-PyP^{5+} twice daily (beginning at 24 hours before radiation and continuing for the duration of the study). Mice were anesthetized with isofluorane, bodies were shielded, and tumors were irradiated for three days with one Gy/day on days 2 to 4 XRAD-320 (Precision X-Ray). Tumors were measured by calipers twice weekly, and tumor volumes were calculated by V = (short $axis^2$ × long axis × 3.14)/6.

Analysis of MnTnBuOE-2-PyP^{5+} in mouse tissue *LC–MS/MS*

Quantitative analysis of MnTnBuOE-2-PyP^{5+} in tissue was performed on a Shimadzu 20A series HPLC–Applied Biosystems MDS Sciex4000 QTrap tandem mass spectrometer at the PK/PD BioAnalytical Duke Cancer Institute Shared Resource. The analysis was performed as reported (13), except that deuterated analogue was used as internal standard.

MRI, image analysis, and quantitation

Magnetic susceptibility images of the brains (n = 3 per group) were acquired at three months after RT and quantified as reported previously (30). Briefly, all images were acquired using a 9.4 T (400 MHz) 89 mm vertical bore Oxford magnet with shielded coil of 2,200 mT/m. The system was controlled by an Agilent VnmrJ 3.2 imaging console. A three dimensional (3D) 12-echo spoiled-gradient-recalled-echo sequence was used to map tissue magnetic susceptibility. Imaging parameters were as follows: matrix size = 256 × 128 × 128, field-of-view (FOV) = 22 × 11 × 11 mm^3, bandwidth = 62.5 kHz, flip angle = 45°, echo time (TE) 1 = 2.4 ms, echo spacing = 2.77 ms, and repetition time (TR) = 100.0 ms. 3D diffusion-weighted images were acquired using a pulsed-gradient spin-echo sequence at a b-value of 1,595 s/mm^2 and with six encoding directions ([1 1 0], [1 0 1], [0 1 1], [1 −1 0], [1 0 −1|, and [0 1 −1]). One nondiffusion-weighted volume was also acquired to calculate the diffusion tensor with a standard linear fitting. The acquisition parameters were as follows: TE = 9 ms, TR = 700 ms, matrix = 192 × 96 × 32, and FOV = 22 × 11 × 11 mm^3. A 3D Fast Fourier Transform algorithm was used to reconstruct images. Quantitative susceptibility map of each brain was computed using the LSQR algorithm as described previously using the software STI Suite (Duke University; refs. 31, 32). Diffusion tensors were calculated as described previously (33). Regions of interest (ROI) in specific brain structures were obtained from a previously defined mouse brain atlas (34). The selected ROIs were transformed back to the original susceptibility maps based on the corresponding transformation matrices obtained through image registration. ROIs that clearly exceeded the tissue boundary were revised accordingly, and susceptibility values were read directly from the original images to avoid interpolation errors. The mean susceptibility in the selected structures was computed.

Histological staining, quantitation, and Western analysis

Three animals from each of the four groups of the neurocognition study were preperfused with paraformaldehyde/glutaraldehyde (4% each) in PBS at three months after RT (35). Whole brains were dissected from the skulls and postfixed overnight in the same fixative. Parasagittal sections were cut 100 μm thick containing the corpus callosum from the same region in each brain. Sections were treated with 2% osmium tetroxide, dehydrated through a series of acetones, embedded in epoxy812, and polymerized (Duke Electron Microscopy Services). One micro meter semi-thin sections were cut, mounted on slides, stained with Toluidine Blue, and blinded for microscopicanalysis. Images of myelinated axon cross-sections were obtained on a Zeiss AxioImager with a 100× objective lens at the Duke Light Microscopy Core Facility. The images were quantified in Adobe Photoshop with the following settings: Image adjustment –invert, black/white -yellow 133, levels 150-1-226, tolerance 32, anti-alias, contig off, point 149 +/− 1. Data were processed blinded before final analysis. Samples of corpus callosum, hippocampus, and cortex were dissected from frozen brains. Lysates were prepared as described (36). Myelin basic protein (Cell Signaling Technology), actin (Sigma), and HRP-goat-anti-mouse (Bio-Rad) antibodies were used with enhanced chemoluminescence (Pierce) for visualization of target proteins. Bands were quantified by Image J and normalized to actin.

Clonogenic assays

LN-18 and LN-229 cells [STR verification by ATCC on December 12, 2011, and June 24, 2012, respectively and cells were used within 6 months of thaw (2012)] were plated in six-well plates at a density of 250 cells per well and treated +/− 50 nmol/L MnTnBuOE-2-PyP^{5+} one day before irradiation. Appropriate plates were irradiated with the indicated dose with an XRAD-320 (Precision X-Ray). Media +/− MnTnBuOE-2-PyP^{5+} were replaced following irradiation. Cultures were allowed to grow for 8 to 9 days and then stained and counted as described (37).

Statistical methods

Behavioral data were assessed with SPSS 20 (IBM SPSS Statistics). The rotorod, novel object recognition, and Morris water maze data were subjected to repeated measures ANOVA (RMA-NOVA) using a within-subjects effect for repeated measures within each test and a between-subject effects of treatment. For the rotorod, water maze, and novel object recognition tasks, the within-subject effects were trial number, test day, and test phase (training/STM/LTM), respectively. Because the fear conditioning tests used separate cohorts of mice for the context and cued tests, ANOVA was used to examine differences between treatments for context testing. For cued fear conditioning, a RMANOVA was used to assess the within-subject effects for the two phases of testing (pretone and tone), among the four treatment conditions. For the wheel running experiment, differences between treatments for revolutions over the 24 hours were examined with ANOVA. *A posteroti* comparisons were conducted with Bonferroni-corrected pairwise comparisons. All data are presented as mean and SEMs; a $P < 0.05$ was considered significant.

For the tumor growth delay study, a mixed effects repeated measures model that assumed an autoregressive correlation structure among repeated measures of log tumor volume within an

animal was used to compare growth patterns among the 4 treatment arms. The analysis included a main effect for arm and assumed the same y-intercept in all arms.

All other statistical methods are described in Results or figure legends.

Results and Discussion

Schedule of mouse groups for imaging and neurocognition studies

Four groups of mice were treated as described in Fig. 1B. At three months after sham/RT, mice were randomly divided and allocated to conduct MR1 (n = 3 per group), histology (n = 3 per group), drug level measurements (n = 2 per group), and neurocognitive/activity testing (n = 20 per group).

Measurement of MnTnBuOE-2-PyP^{5+} levels in tissue

At three months after RT, but 1 month after the last MnTnBuOE-2-PyP^{5+} injection, tissues from the brain and liver of two mice were processed for mass spectroscopy measurement from the two groups treated with MnTnBuOE-2-PyP^{5+}. Concentrations in brain were quantified at 25 to 30 nmol/L, whereas liver concentrations were in the range of 5,000 nmol/L (Table 1).

MRI of white matter tracts in brain

Qualitatively, the corpus callosum demonstrated less diamagnetic susceptibility in the saline/RT group (Fig. 2A) than the MnTnBuOE-2-PyP^{5+}/RT group at three months after RT (Fig. 2B). Brighter intensity (more negative) in the white matter correlates to more diamagnetic susceptibility and, therefore, more myelination. In addition, we observed a decreased DTI fractional anisotropy and radial diffusivity in the saline/RT over the MnTnBuOE-2-PyP^{5+}/RT group, further suggesting myelin loss. The mean susceptibility in both the corpus callosum and hippocampal commissure was 2-fold more diamagnetic in the MnTnBuOE-2-PyP^{5+} group compared with the saline/GR group: −0.0064 ppm versus −0.0038 ppm in corpus callosum and −0.0068 ppm versus −0.0032 ppm in hippocampal commissure (Fig. 2C). There was a trend toward statistical significance (P = 0.0929). No clear differences were observed in anterior commissure or cerebellum. MRI scans of mouse brains have limited sensitivity at the millimeter scale; therefore, the significance between groups was difficult to demonstrate.

Histological evaluation of myelinated axons in the corpus callosum

To verify trends observed with MRI, we performed histological analysis of this tissue. Brain sections from all treatment groups were analyzed for alterations in axon density in the midsagittal plane of the corpus callosum. Representative sections were photographed (Fig. 3A–D) and axons were counted using a predetermined standard set of image analysis parameters using Photoshop. Quantification of axon numbers per field revealed that the loss of axons after treatment was significant [ANOVA $F_{(3, 11)}$, P = 0.04]. However, this loss was mitigated in the MnTnBuOE-2-PyP^{5+}/RT group (Fig. 3E), indicating a radioprotective effect of MnTnBuOE-2-PyP^{5+} on axons, myelinating oligodendrocytes, or both. Western analysis of myelin within the corpus callosum demonstrated the strongest decrease of myelin signal

in the saline/RT group (Supplementary Fig. S1) with the loss of myelin likely due to the loss of overall neurons.

Neurobehavioral testing

A RMANOVA for performance on the accelerating rotorod on day 1 found a significant effect of test trial [$F_{(3,81)} = 18.115$, $P < 0.001$], but the test trial by treatment interaction was not significant. All animals showed motor learning across trials, with no differences observed among the different treatment conditions across trials (Fig. 4A). RMANOVA for responses on the steady-speed rotorod on day 2 noted that performance across test trials was not significant; however, the test trial by treatment interaction was significant [$F_{(3,81)} = 2.301$, $P < 0.042$; Fig. 4B]. Bonferroni-corrected pairwise comparisons demonstrated that on trials 3 and 4, the saline controls had longer latencies to fall relative to the saline/RT animals (ps < 0.034). Although not significant, mice receiving MnTnBuOE-2-PyP^{5+}/RT had longer latencies to fall than the saline/RT-treated mice. Motor performance was also assessed by wheel running activity. Analyses of wheel running activity by ANOVA determined that treatment condition was significant [$F_{(2,14)} = 3.221$, $P < 0.036$; Fig. 4C]. Bonferroni comparisons showed that that the total activity by the MnTnBuOE-2-PyP^{5+}/RT group was higher than the saline/RT animals ($P < 0.034$), and the activity of this latter group was marginally lower than that for the saline animals ($P < 0.079$). No differences were found between the mice that received saline and those that were treated with MnTnBuOE-2-PyP^{5+}/RT. Together, the rotorod and wheel running activity show that MnTnBuOE-2-PyP^{5+} can protect mice from the effects of RT.

Mice were also examined for cognitive functioning in the Morris water maze, novel object recognition, and fear conditioning tests. Spatial memory and plasticity of responding were examined in the Morris water maze. An omnibus RMANOVA found a significant effect of test day [$F_{(11,396)} = 65.397$, $P < 001$]; the test day by treatment interaction was not significant (Supplementary Fig. S2A and S2B). Hence, all mice acquired the task and successfully found the hidden platform when it was moved to a new location. These data show that spatial memory and plasticity of responding were not distinguished by treatment assignment. Episodic memory was examined in the novel object recognition memory test. A RMANOVA revealed the main effect of test phase [i.e., training, STM, LTM; $F_{(2,70)} = 18.641$, $P < 0.001$], and the test phase by treatment interaction was significant [$F_{(3,35)} = 3.318$, $P < 0.031$; Supplementary Fig. S2C]. Bonferroni tests observed that all animals regardless of treatment condition had a marked preference for the novel object during the STM and LTM tests compared with preferences at training (ps < 0.050). Nonetheless, no group differences were discerned during training or the LTM test. However, during the STM test, mice that received MnTnBuOE-2-PyP^{5+} showed a stronger preference for the novel object than the saline/RT mice and MnTnBuOE-2-PyP^{5+}/RT animals (ps < 0.040). Mice administered with MnTnBuOE-2-PyP^{5+} alone did not differ from the saline controls. Although novel object preference was lower in the two groups of irradiated mice (saline/RT or MnTnBuOE-2-PyP^{5+}/RT) relative to the saline controls, this difference was not statistically significant. These differences in episodic memory function cannot be attributed to neophobia because no differences were found among the animals in object exploration during any phase of training/testing (Supplementary Fig. S2D, S2F, and S2F). Together, our

results indicate that mice given MnP alone have an enhancement in STM compared with the irradiated animals. Because no group differences were observed at LTM, it appears that irradiation may slow the consolidation of episodic memory processes. Mice were examined also in conditioned fear. ANOVA found no significant differences in freezing behaviors in the context test, indicating that hippocampal-mediated processes of emotional memory were intact (Supplementary Fig. S2G). For the cued tests, a RMANOVA reported a significant main effect of test phase [i.e., non-CS vs. CS; $F_{(1,16)} = 51.466$, $P < 0.001$]; however, the test phase by treatment interaction was not significant (Supplementary Fig. S2H). Bonferroni corrections demonstrated that freezing behaviors were significantly enhanced for all treatment groups during the CS than during the non-CS phase of testing ($ps < 0.024$). These findings show that irradiation or treatment with MnTnBuOE-2-PyP^{5+} did not affect fear memories.

MnTnBuOE-2-PyP^{5+} effect on glioblastoma multiforme growth in mouse xenograft model

Flank tumor growth of D-245 MG glioblastoma cells implanted nude mice was evaluated using a mixed-effects model (Fig. 5). The rate of tumor growth compared with the control group was significantly less in the radiation dose group ($P = 0.0178$) group and the MnTnBuOE-2-PyP^{5+}/RT group ($P < 0.0001$). The following pair-wise comparisons of the active treatment groups were significantly different: (i) MnTnBuOE-2-PyP^{5+}/RT and MnTnBuOE-2-PyP^{5+} ($P < 0.0001$), (ii) RT and MnTnBuOE-2-PyP^{5+} ($P = 0.0029$), and (iii) MnTnBuOE-2-PyP^{5+}/RT and RT ($P = 0.0088$). Although RT demonstrated a significantly reduced tumor growth compared with saline, the combination of MnTnBuOE-2-PyP^{5+} and RT produced a further significant reduction in tumor growth when compared with RT only. Thus, MnTnBuOE-2-PyP^{5+} may have dual roles toward normal (protective) and tumortissue (detrimental). Such potential properties would make MnTnBuOE-2-PyP^{5+} an attractive adjunct therapy with RT.

MnTnBuOE-2-PyP^{5+} effects on tumor cells *in vitro*

IN-18 and LN-229 glioblastoma cell lines were irradiated *in vitro* in the absence or presence of 50 nmol/L. MnTnBuOE-2-PyP^{5+} and radiosensitivity was assessed by clonogenic survival assays (Supplementary Fig. S3). MnTnBuOE-2-PyP^{5+} showed no significant protective effect on survival of either cell line at a drug concentration similar to what was observed in brain (Table 1). MnTnBuOE-2-PyP^{5+} provided no difference in tumor cell line survival in the presence or absence of RT.

MnTnBuOE-2-PyP^{5+} uptake in brain

A critical feature of the neuroprotective effects of MnTnBuOE-2-PyP^{5+} is its ability to cross the BBB and accumulate in brain and brain mitochondria (14). The high lipophilicity of alkoxyalkyl groups attached to the central porphyrin structure permits access of this compound to the CNS (8, 14). At the end of the study, MnTnBuOE-2-PyP^{5+} had accumulated in the brain at 25 to 30 nmol/L concentrations. The liver accumulated low micromolar amounts of MnTnBuOE-2-PyP^{5+} and may serve as a depot of the compound, constantly providing the rest of the body with access to the drug through the bloodstream. Interestingly, a previous characterization of MnTnBuOE-2-PyP^{5+} distribution within the

brain substructures after one week of daily injections revealed a disproportionate accumulation of MnTnBuOE-2-PyP^{5+} within the hippocampus (85 nmol/L) as opposed to the cortex (14 nmol/L; ref. 38). The hippocampus is an important anatomical structure for learning and memory, and it contains a neurogenic zone critical for generation of new neurons. Therefore, protection from radiation is essential to avoid long-term cognitive dysfunction (39–41). If MnTnBuOE-2-PyP^{5+} concentrated within the hippocampus in this study, this structure may have a higher capacity to benefit from the protection against radiation-induced damage relative to other brain areas. Our preliminary histological analyses of the hippocampus and behavioral analyses of spatial, episodic, and fear memories that rely upon intact hippocampal function could find no evidence that MnTnBuOE-2-PyP^{5+} treatment was deleterious to this brain area. Regardless of its distribution patterns in the brain, MnTnBuOE-2-PyP^{5+} demonstrated the ability to preserve both brain structure and function following RT.

Axonal radioprotection by MnTnBuOE-2-PyP^{5+}

The primary radioprotective effect of MnTnBuOE-2-PyP^{5+} toward RT-induced white matter loss was observed in the corpus callosum. MR imaging demonstrated evident visual changes at the margins of neighboring corpus callosum and gray matter regions between irradiated +/− MnTnBuOE-2-PyP^{5+} groups. These data agreed with previous work showing a reduction of corpus callosal fractional anisotrophy in patients with pediatric medulloblastoma (42). Further histological evaluation verified a significant difference in axon number among the four groups. Therefore, the deficiency of MR signal in irradiated brains was due to loss of axons and their myelin and the less ordered radial diffusivity of water along these myelinated nerve bundles. The antioxidant properties of MnTnBuOE-2-PyP^{5+} likely prevented neuronal cell death in the irradiated corpus callosum, preserving the brain circuitry. In stroke models of oxidative stress protection in brain by MnTE-2-PyP^{5+} and MnTnHex-2-PyP^{5+}, both porphyrin compounds reduced oxidative stress by either 8-hydroxy-2′-deoxyguanosine or NF-κB markers (43–45). Because MnTnBuOE-2-PyP^{5+} operates with nearly identical SOD-like properties and peroxynitrite reduction, we believe MnTnBuOE-2-PyP^{5+} does protect against RT-induced white matter loss by reducing oxidative stress and subsequent inflammatory signaling (8). A previous study used a 12.5-fold higher radiation dose (100 Gy) delivered to rat brain in the presence of MnTDE-2-ImP^{5+}, Mn(III) tetrakis[*N*,*N*′-diethylimidazolium-2-yl)porphyrin, and the investigators also noted a rescue of white matter (46). There may be a large range of radiation doses that can be modulated by MnTnBuOE-2-PyP^{5+} treatment.

Neurocognitive rescue by MnTnBuOE-2-PyP^{5+}

The radiation-induced loss of brain function was indicated in neurobehavioral analyses. The rotorod tests motor performance and learning and are governed by the cerebellum and motor cortex. Mice treated with whole-brain RT may have neurological impairments that manifest as ataxia and, subsequently, deficits in rotorod performance (47). In addition, motor learning can be evaluated across several rotorod trials (48). Our rotorod data showed increased learning of the saline control group over the four steady-state longitudinal trials. In the steady-speed tests, the saline/RT group was the lowest performing group compared with the saline controls on trials 3 and 4 (Fig. 4B). The MnTnBuOE-2-PyP^{5+}/RT group performed

between these two groups, showing rescue of RT-induced deficits. These deficits on this rotorod task suggest that RT may produce interruptions in the circuitry that links the cerebellum, motor cortex, and/or motor neuron pathways. Notably, we observed no appreciable differences in cerebellar white matter by MRI between the irradiated groups. Therefore, radiation-induced imperfections in the corpus callosum may sever important linkages between the left and right hemispheres, leading to perturbations in coordination, balance, motor learning, or combinations of these issues.

The running wheel test evaluated spontaneous activity of the mice. These data showed reduced performance in the saline/RT group that was ameliorated by MnTnBuOE-2-PyP^{5+}. Interestingly, three of five mice in the saline/RT group and one saline mouse chose not to run in the wheel on day 1. Those in the saline/RT group that ran did so approximately 66% of the MnTnBuOE-2-PyP^{5+}/RT group. The reduced performance in the saline/RT group likely was not the result of neophobia to the running wheel because the wheel was left in the cage for 24 hours. Rather, coordination, balance, or motivational barriers had to be overcome. As hypothesized, MnTnBuOE-2-PyP^{5+} treatment relieved the RT-induced performance impairment on this test.

Possible dual role of MnTnBuOE-2-PyP^{5+} in RT of brain cancers

Although MnTnBuOE-2-PyP^{5+} protected normal brain tissue, tumor cells and tumors were not protected by it. In general, tumor cells have higher oxidative stress level than normal cells due to an imbalance between antioxidant capacity and ROS levels (18, 19) and, therefore, may respond more robustly to antioxidant therapies. As described above, however, our previous porphyrin analogues did not preserve tumor cell growth *in vitro* or *in vivo* but, in fact, they did sensitize tumors to radiation *in vivo* (8, 9, 11, 20–22). Treatment of tumor cells or tumors with MnTnBuOn-2-PyP^{5+} likewise demonstrated no protective advantage and, like the earlier analogues, sensitized flank tumors to radiation. The difference in redox states between normal and tumor cells permits these porphyrins to reduce not only ROS in tumors, but also suppress the NF-κB and HIF1α signaling pathways triggered by the excess ROS that give tumors a growth advantage (8, 10, 11). Thus, the outcomes between normal and tumor tissue result in survival versus death, respectively (Supplementary Fig. S4), Furthermore, MnTE-2-PyP^{5+} has been shown to act in a pro-oxidant fashion to specifically inactivate NF-κB by direct chemical modification when combined with dexamethasome therapy of lymphoma cells (49). Thus, such a mechanism can also explain our therapeutically beneficial results of MnTnBuOE-2-PyP^{5+} treatment toward both normal and tumor tissues.

Conclusions

As a first *in vivo* test on healthy brain tissue, MnTnBuOE-2-PyP^{5+} clearly counteracted the negative effects of cranial irradiation. Its ability to efficiently cross the BBB and accumulate in the brain makes it ideal to neutralize RT-induced ROS and downstream inflammatory signaling generated after exposure to RT (8, 9, 14). As a result, the white matter preservation demonstrated by MnTnBuOE-2-PyP^{5+} correlates with evidence of neuroprotective function in the neurobehavioral tests described herein. MnTnBuOE-2-PyP^{5+} also exhibited

radiosensitizing properties to slow glioblastoma tumor growth in flank tumor growth assays. The addition of MnTnBuOE-2-PyP^{5+} to radiation therapy for brain tumors will be likely beneficial in preserving healthy brain structure and function while simultaneously antagonizing tumor survival.

Supplementary Material

Refer to Web version on PubMed Central for supplementary material.

Acknowledgments

The authors thank the Pediatric Brain Tumor Foundation and Preston Robert Tisch Brain Tumor Center at Duke for support and cell lines. They also thank the Duke Cancer Institute Animal Pathology Core, Duke Center for *In Vivo* Microscopy (P41EB0T5897), Duke Electron Microscopy Services, and Light Microscopy Core Facility for pathologic and microscopic expertise and the Duke Mouse Behavioral and Neuroendocrine Analysis Core Facility for help with behavioral testing.

Grant Support

This study was supported by the Pediatric Brain Tumor Foundation Institute and Preston Robert Tisch Brain Tumor Center at Duke, C. Liu was supported in part by the National Institutes of Health through grant R01 MH096979 and the National Multiple Sclerosis Society through grant RG4723.

References

1. Greene-Schloesser D, Robbins ME, Peiffer AM, Shaw EC, Wheeler KT, Chan MD. Radiation-induced brain injury: a review. Front Oncol. 2012; 2:73. [PubMed: 22833841]
2. Padovani L, Andre N, Constine LS, Muracciole X. Neurocognitive function after radiotherapy for paediatric brain tumours. Nat Rev Neurol. 2012; 8:578–588. [PubMed: 22964509]
3. Askins MA, Moore BD 3rd. Preventing neurocognitive late effects in childhood cancer survivors. J Child Neurol. 2008; 23:1160–1171. [PubMed: 18952582]
4. Ullrich NJ, Embry L. Neurocognitive dysfunction in survivors of childhood brain tumors. Semin Pediatr Neurol. 2012; 19:35–42. [PubMed: 22641074]
5. Fuchs-Tarlovsky V. Role of antioxidants in cancer therapy. Nutrition. 2013; 29:15–21. [PubMed: 22784609]
6. Manda K, Ueno M, Moritake T, Anzai K. Radiation-induced cognitive dysfunction and cerebellar oxidative stress in mice: protective effect of alpha-lipoic acid. Behav Brain Res. 2007; 177:7–14. [PubMed: 17145083]
7. Oh SB, Park HR, Jang YJ, Choi SY, Son TC, Lee J. Baicalein attenuates impaired hippocampal neurogenesis and the neurocognitive deficits induced by gamma-ray radiation. Br J Pharmacol. 2013; 168:421–431. [PubMed: 22891631]
8. Batinic-Haberle I, Tovmasyan A, Roberts ER, Vujaskovic Z, Leong KW, Spasojevic I. SOD therapeutics: latest insights into their structure-activity relationships and impact on the cellular redox-based signaling pathways. Antioxid Redox Signal. 2014; 20:2372–2415. [PubMed: 23875805]
9. Tovmasyan A, Sheng H, Weitner T, Arulpragasam A, Lu M, Warner DS, et al. Design, mechanism of action, bioavailability and therapeutic effects of mn porphyrin-based redox modulators. Med Princ Pract. 2013; 22:103–130. [PubMed: 23075911]
10. Moeller BJ, Cao Y, Li CY, Dewhirst MW. Radiation activates HIF-1 to regulate vascular radiosensitivity in tumors: role of reoxygenation, free radicals, and stress granules. Cancer Cell. 2004; 5:429–441. [PubMed: 15144951]
11. Rabbani ZN, Spasojevic I, Zhang X, Moeller BJ, Haberle S, Vasquez-Vivar J, et al. Antiangiogenic action of redox-modulating Mn(III) meso-tetrakis(N-ethylpyridinium-2-yl)porphyrin, MnTE-2-PyP(5+), via suppression of oxidative stress in a mouse model of breast tumor. Free Radic Biol Med. 2009; 47:992–1004. [PubMed: 19591920]

12. Aitken JB, Shearer EL, Giles NM, Lai B, Vogt S, Reboucas JS, et al. Intracellular targeting and pharmacological activity of the superoxide dismutase mimics MnTE-2-PyP5+ and MnTnHex-2-PyP5+ regulated by their porphyrin ring substituents. Inorg Chem. 2013; 52:4121–4123. [PubMed: 23551184]
13. Weitner T, Kos I, Sheng H, Tovmasyan A, Reboucas JS, Fan P, et al. Comprehensive pharmacokinetic studies and oral bioavailability of two Mn porphyrin-based SOD mimics. MnTE-2-PyP5+ and MnTnHex-2-PyP5+ Free Radic Biol Med. 2013; 58:73–80. [PubMed: 23328731]
14. Rajic Z, Tovmasyan A, Spasojevic I, Sheng H, Lu M, Li AM, et al. A new SOD mimic, Mn(III) ortho N-butoxyethylpyridylporphyrin, combines superb potency and lipophilicity with low toxicity. Free Radic Biol Med. 2012; 52:1828–1834. [PubMed: 22336516]
15. Vujaskovic Z, Batinic-Haberle I, Rabbani ZN, Feng QF, Kang SK, Spasojevic I, et al. A small molecular weight catalytic metalloporphyrin antioxidant with superoxide dismutase (SOD) mimetic properties protects lungs from radiation-induced injury. Free Radic Biol Med. 2002; 33:857–863. [PubMed: 12208373]
16. Gauter-Fleckenstein B, Fleckenstein K, Owzar K, Jiang C, Batinic-Haberle I, Vujaskovic Z. Comparison of two Mn porphyrin-based mimics of superoxide dismutase in pulmonary radioprotection. Free Radic Biol Med. 2008; 44:982–989. [PubMed: 18082148]
17. Lee JH, Park JW. A manganese porphyrin complex is a novel radiation protector. Free Radic Biol Med. 2004; 37:272–283. [PubMed: 15203198]
18. Buettner GR. Superoxide dismutase in redox biology: the roles of superoxide and hydrogen peroxide. Anticancer Agents Med Chem. 2011; 11:341–346. [PubMed: 21453242]
19. Zhao W, Robbins ME. Inflammation and chronic oxidative stress in radiation-induced late normal tissue injury: therapeutic implications. Curr Med Chem. 2009; 16:130–143. [PubMed: 19149566]
20. Gridley DS, Makinde AY, Luo X, Rizvi A, Crapo JD, Dewhirst MW, et al. Radiation and a metalloporphyrin radioprotectant in a mouse prostate tumor model. Anticancer Res. 2007; 27:3101–3109. [PubMed: 17970050]
21. Moeller BJ, Batinic-Haberle I, Spasojevic I, Rabbani ZN, Anscher MS, Vujaskovic Z, et al. A manganese porphyrin superoxide dismutase mimetic enhances tumor radioresponsiveness. Int J Radiat Oncol Biol Phys. 2005; 63:545–552. [PubMed: 16168847]
22. Keir ST, Dewhirst MW, Kirkpatrick JP, Bigner DD, Batinic-Haberle I. Cellular redox modulator, ortho Mn(III) meso-tetrakis(N-n-hexylpyridinium-2-yl)porphyrin, MnTnHex-2-PyP(5+) in the treatment of brain tumors. Anticancer Agents Med Chem. 2011; 11:202–212. [PubMed: 21291403]
23. Mehrotra S, Pecaut MJ, Freeman TL, Crapo JD, Rizvi A, Luo-Owen X, et al. Analysis of a metalloporphyrin antioxidant mimetic (MnTE-2-PyP) as a radiomitigator: prostate tumor and immune status. Technol Cancer Res Treat. 2012; 11:447–457. [PubMed: 22475066]
24. Porton B, Rodriguiz RM, Phillips LE, Gilbert JWt, Feng J, Greengard P, et al. Mice lacking synapsin III show abnormalities in explicit memory and conditioned fear. Genes Brain Behav. 2010; 9:257–268. [PubMed: 20050925]
25. Wang X, McCoy PA, Rodriguiz RM, Pan Y, Je HS, Roberts AC, et al. Synaptic dysfunction and abnormal behaviors in mice lacking major isoforms of Shank3. Hum Mol Genet. 2011; 20:3093–3108. [PubMed: 21558424]
26. Ribar TJ, Rodriguiz RM, Khiroug L, Wetsel WC, Augustine GJ, Means AR. Cerebellar defects in Ca2+/calmodulin kinase IV-deficient mice. J Neurosci. 2000; 20:RC107. [PubMed: 11069976]
27. Kolstad AM, Rodriguiz RM, Kim CJ, Hale LP. Effect of pain management on immunization efficacy in mice. J Am Assoc Lab Anim Sci. 2012; 51:448–457. [PubMed: 23043810]
28. Rodriguiz, RM.; Wetsel, WC. Assessments of cognitive deficits in mutant mice. In: Levin, ED.; Buccafusco, JJ., editors. Animal models of cognitive impairment. Boca Raton, FL: CRC Press; 2006. p. 223-282.
29. Wetsel WC, Rodriguiz RM, Guillemot J, Rousselet E, Essalmani R, Kim IH, et al. Disruption of the expression of the proprotein convertase PC7 reduces BDNF production and affects learning and memory in mice. Proc Natl Acad Sci U S A. 2013; 110:17362–17367. [PubMed: 24101515]

30. Liu C, Li W, Johnson GA, Wu B. High-field (9.4 T) MRI of brain dysmyelination by quantitative mapping of magnetic susceptibility. Neuroimage. 2011; 56:930–938. [PubMed: 21320606]
31. Li W, Wu B, Liu C. Quantitative susceptibility mapping of human brain reflects spatial variation in tissue composition. Neuroimage. 2011; 55:1645–1656. [PubMed: 21224002]
32. Li W, Avram AV, Wu B, Xiao X, Liu C. Integrated Laplacian-based phase unwrapping and background phase removal for quantitative susceptibility mapping. NMR Biomed. 2014; 27:219–227. [PubMed: 24357120]
33. Basser PJ, Pierpaoli C. Microstructural and physiological features of tissues elucidated by quantitative-diffusion-tensor MRI. J Magn Reson B. 1996; 111:209–219. [PubMed: 8661285]
34. Badea A, Ali-Sharief AA, Johnson GA. Morphometric analysis of the C57BL/6J mouse brain. Neuroimage. 2007; 37:683–693. [PubMed: 17627846]
35. Kuo CT, Mirzadeh Z, Soriano-Navarro M, Rasin M, Wang D, Shen J, et al. Postnatal deletion of Numb/Numblike reveals repair and remodeling capacity in the subventricular neurogenic niche. Cell. 2006; 127:1253–1264. [PubMed: 17174898]
36. Weitzel DH, Chambers J, Haystead TA. Phosphorylation-dependent control of ZIPK nuclear import is species specific. Cell Signal. 2011; 23:297–303. [PubMed: 20854903]
37. Landon CD, Benjamin SF, Ashcraft KA, Dewhirst MW. A role for the copper transporter Ctrl in the synergistic interaction between hyperthermia and cisplatin treatment. Int J Hyperthermia. 2013; 29:528–538. [PubMed: 23879689]
38. Batinic-Haberle I, Tovmasyan A, Weitner T, Rajic Z, Keir ST, Huang T-T, et al. Mechanistic Considerations of the Therapeutic Effects of Mn Porphyrins, Commonly Regarded as SOD Mimics, in Anticancer Therapy: Lessons from Brain and Lymphoma Studies. Free Radical Bio Med. 2013; 65(Supplement 2):S120–S121.
39. Acharya MM, Christie LA, Lan ML, Donovan PJ, Cotman CW, Fike JR, et al. Rescue of radiation-induced cognitive impairment through cranial transplantation of human embryonic stem cells. Proc Natl Acad Sci U S A. 2009; 106:19150–19155. [PubMed: 19901336]
40. Rao AA, Ye H, Decker PA, Howe CL, Wetmore C. Therapeutic doses of cranial irradiation induce hippocampus-dependent cognitive deficits in young mice. J Neurooncol. 2011; 105:191–198. [PubMed: 21499912]
41. Kumar M, Haridas S, Trivedi R, Khushu S, Manda K. Early cognitive changes due to whole body gamma-irradiation: a behavioral and diffusion tensor imaging study in mice. Exp Neurol. 2013; 248:360–368. [PubMed: 23769909]
42. Mabbott DJ, Noseworthy MD, Bouffet E, Rockel C, Laughlin S. Diffusion tensor imaging of white matter after cranial radiation in children for medulloblastoma: correlation with IQ. Neuro Oncol. 2006; 8:244–252. [PubMed: 16723629]
43. Mackensen GB, Patel M, Sheng H, Calvi CL, Batinic-Haberle I, Day BJ, et al. Neuroprotection from delayed postischemic administration of a metalloporphyrin catalytic antioxidant. J Neurosci. 2001; 21:4582–4592. [PubMed: 11425886]
44. Sheng H, Spasojevic I, Tse HM, Jung JY, Hong J, Zhang Z, et al. Neuroprotective efficacy from a lipophilic redox-modulating Mn(III) N-Hexylpyridylporphyrin, MnTnHex-2-PyP: rodent models of ischemic stroke and subarachnoid hemorrhage. J Pharmacol Exp Ther. 2011; 338:906–916. [PubMed: 21652782]
45. Sheng H, Yang W, Fukuda S, Tse HM, Paschen W, Johnson K, et al. Long-term neuroprotection from a potent redox-modulating metalloporphyrin in the rat. Free Radic Biol Med. 2009; 47:917–923. [PubMed: 19631268]
46. Pearlstein RD, Higuchi Y, Moldovan M, Johnson K, Fukuda S, Gridley DS, et al. Metalloporphyrin antioxidants ameliorate normal tissue radiation damage in rat brain. Int I Radial Biol. 2010; 86:145–163.
47. Karl T, Pabst R, von Horsten S. Behavioral phenotyping of mice in pharmacological and toxicological research. Exp Toxicol Pathol. 2003; 55:69–83. [PubMed: 12940631]
48. Crawley JN. Behavioral phenotyping strategies for mutant mice. Neuron. 2008; 57:809–818. [PubMed: 18367082]

49. Jaramillo MC, Briehl MM, Crapo JD, Batinic-Haberle I, Tome ME. Manganese porphyrin, MnTE-2-PyP5+, Acts as a pro-oxidant to potentiate glucocorticoid-induced apoptosis in lymphoma cells. Free Radic Biol Med. 2012; 52:1272–1284. [PubMed: 22330065]

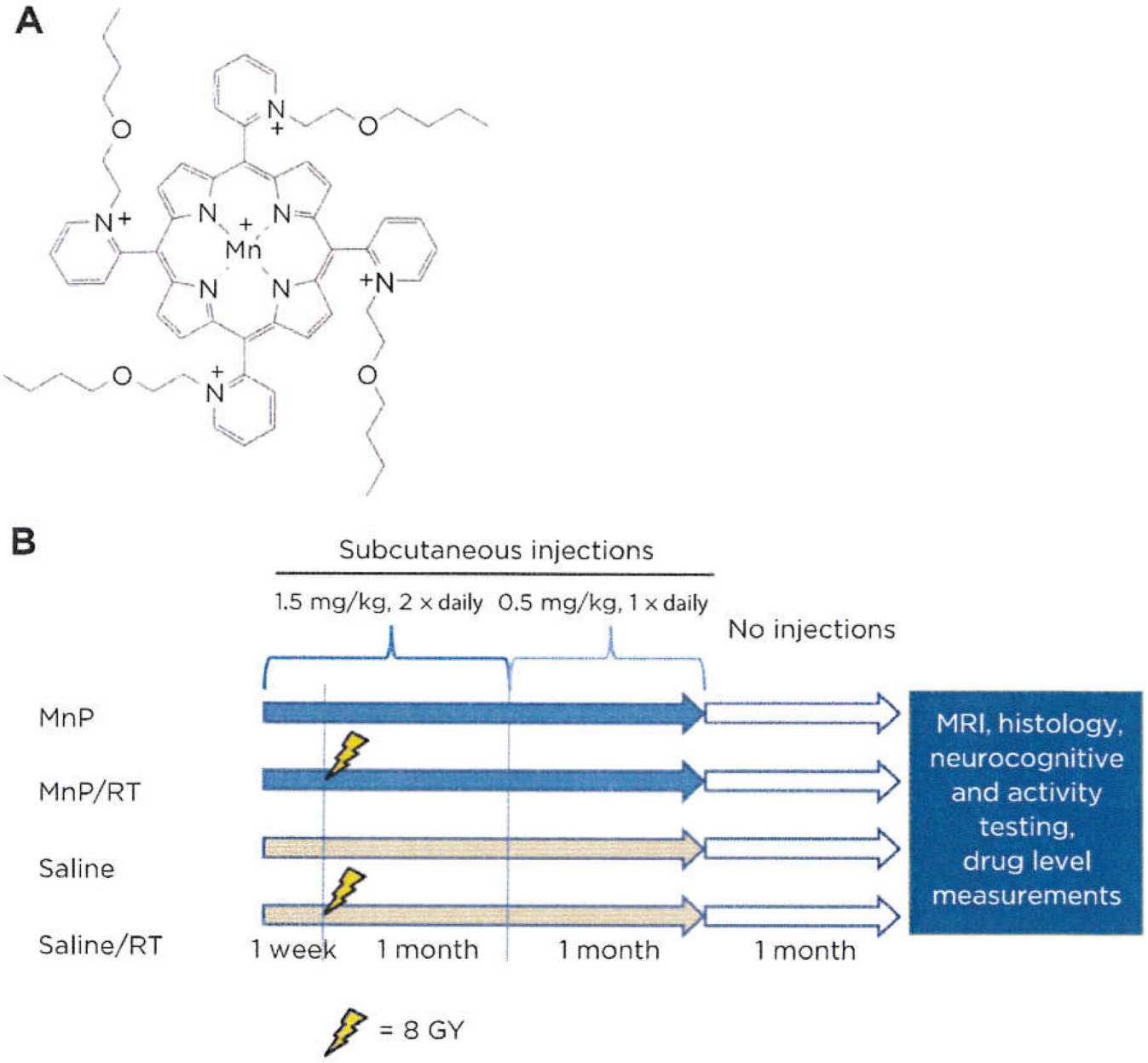

Figure 1.

Porphyrin chemical structure and schedule of the brain radioprotection study. A, chemical structure of MnTnBuOE-2-PyP^{5+}. B, all groups began saline or MnTnBuOE-2-PyP^{5+} dosing one week before and for two months after sham or RT (8 Gy). After three months post-RT, all groups were subjected to imaging, neurocognitive testing, or MnTnBuOE-2-PyP^{5+} tissue analysis.

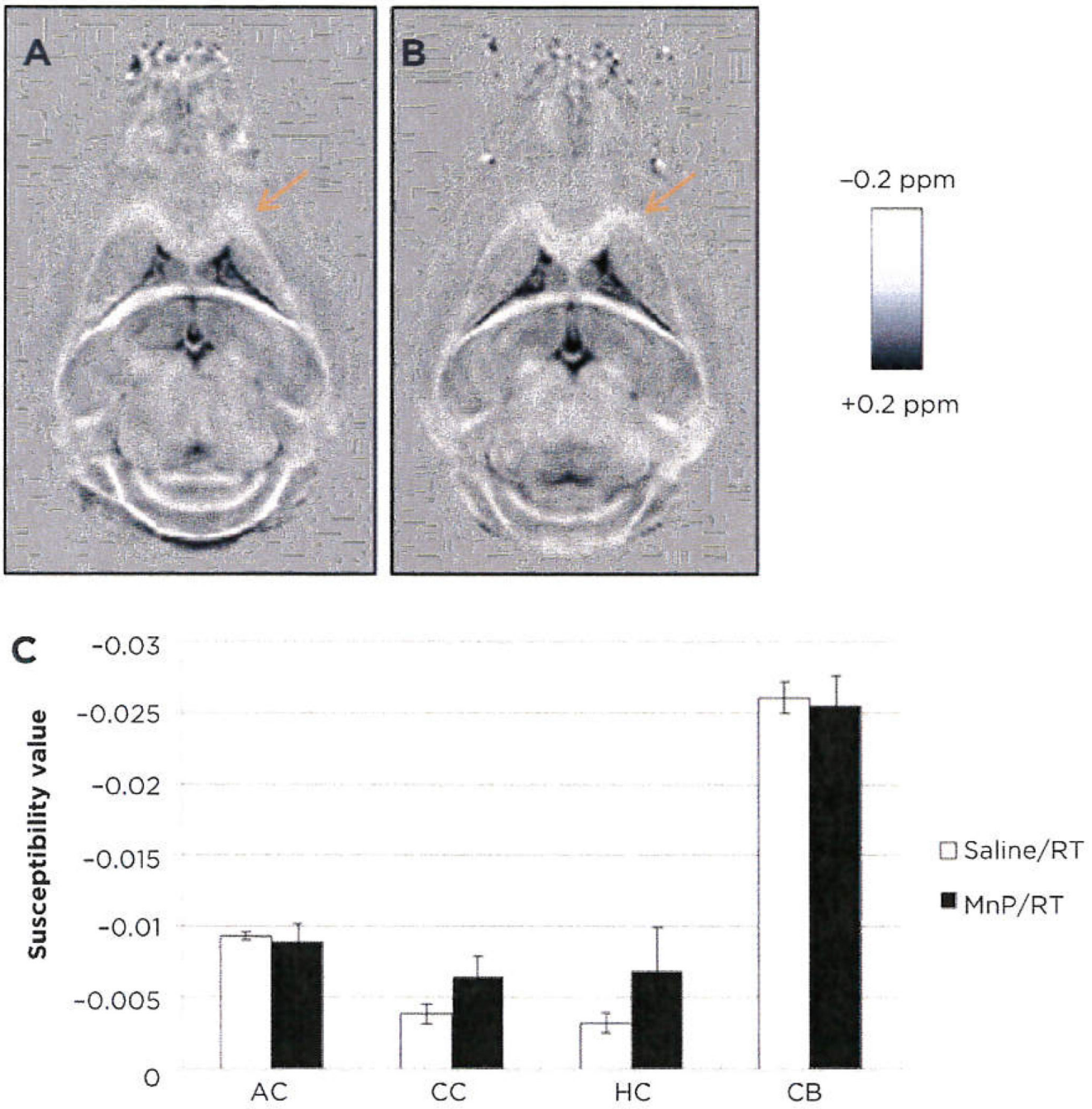

Figure 2.

Magnetic susceptibility mapping of white matter tracts. Quantitative susceptibility maps of saline/RT (A) and MnTnBuOE-2-PyP^{5+}/RT (B) mouse brains (representative images, n = 3). Four white matter tracts from images above were quantitated and statistically analyzed (C: AC, anterior commissure; CC, corpus callosum: HC, hippocampal commissure; CB, cerebellum). Data were analyzed by the Student t test.

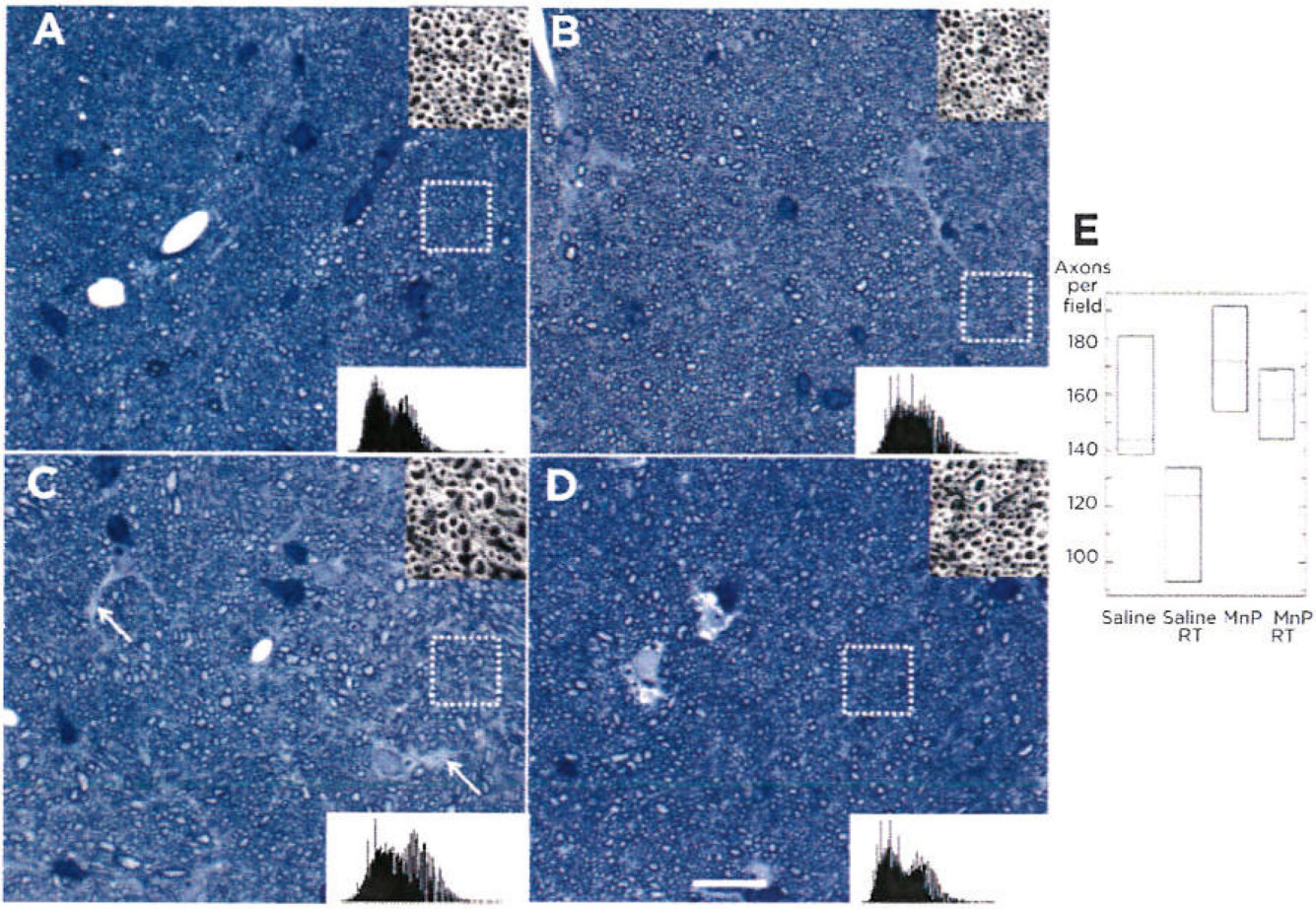

Figure 3.

Histological evaluation of myelinated axons in the corpus callosum. Representative images of toluidine blue-stained midsagittal corpus callosum tissue were imaged by brightfield microscopy (n = 3 mice/group). Saline (A), MnTnBuOE-2-PyP^{5+} (B), saline/RT (C), and MnTnBuOE-2-PyP^{5+}/RT (D). Note the uniform spacing of axons in A, B, and D, but many spaces lacking myelinated axons in C (white arrows) White dotted box identifies inset images (top right), which show one of seven areas within the image that was counted (A–D). Histograms of the entire image are also shown (lower right). Scale bar, 20 μm. E, three images from each mouse underwent automated axon counting that is guantitated in the box graph with 95% confidence intervals. ANOVA analysis of the group resulted in significant differences among the group (P = 0.040).

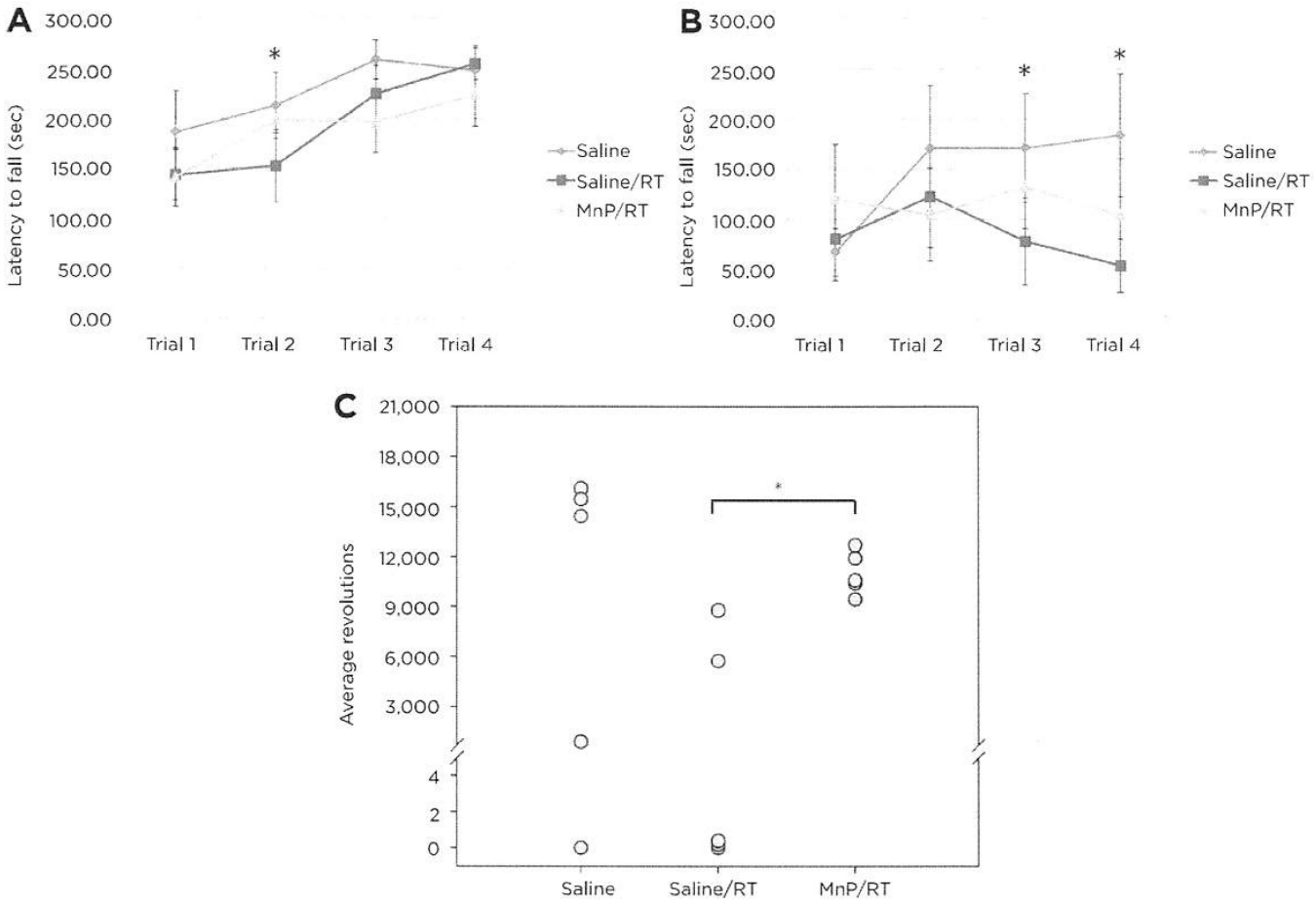

Figure 4.

Neuromotor analyses of mice by rotorod and running wheel. A, accelerating rotorod trials of ten mice per group showed a significant reduction in performance between the saline and saline/RT groups on trial 2 (*, $P = 0.034$). B, steady-state rotorod analyses demonstrated that the saline controls had longer latencies to fall relative to the saline/RT animals on trials 3 and 4 (*, $P = 0.023$, $P = 0.003$. respectively). C. in the voluntary running wheel tests ($n = 5$), total activity on MnTnBuOE-2-PyP^{5+}/RT group was higher than that in the saline/RT animals ($P = 0.034$), and the activity of this latter group was marginally lower than that for the saline animals ($P < 0.079$). Four mice (one from the saline group and three from the saline/RT group) did not run.

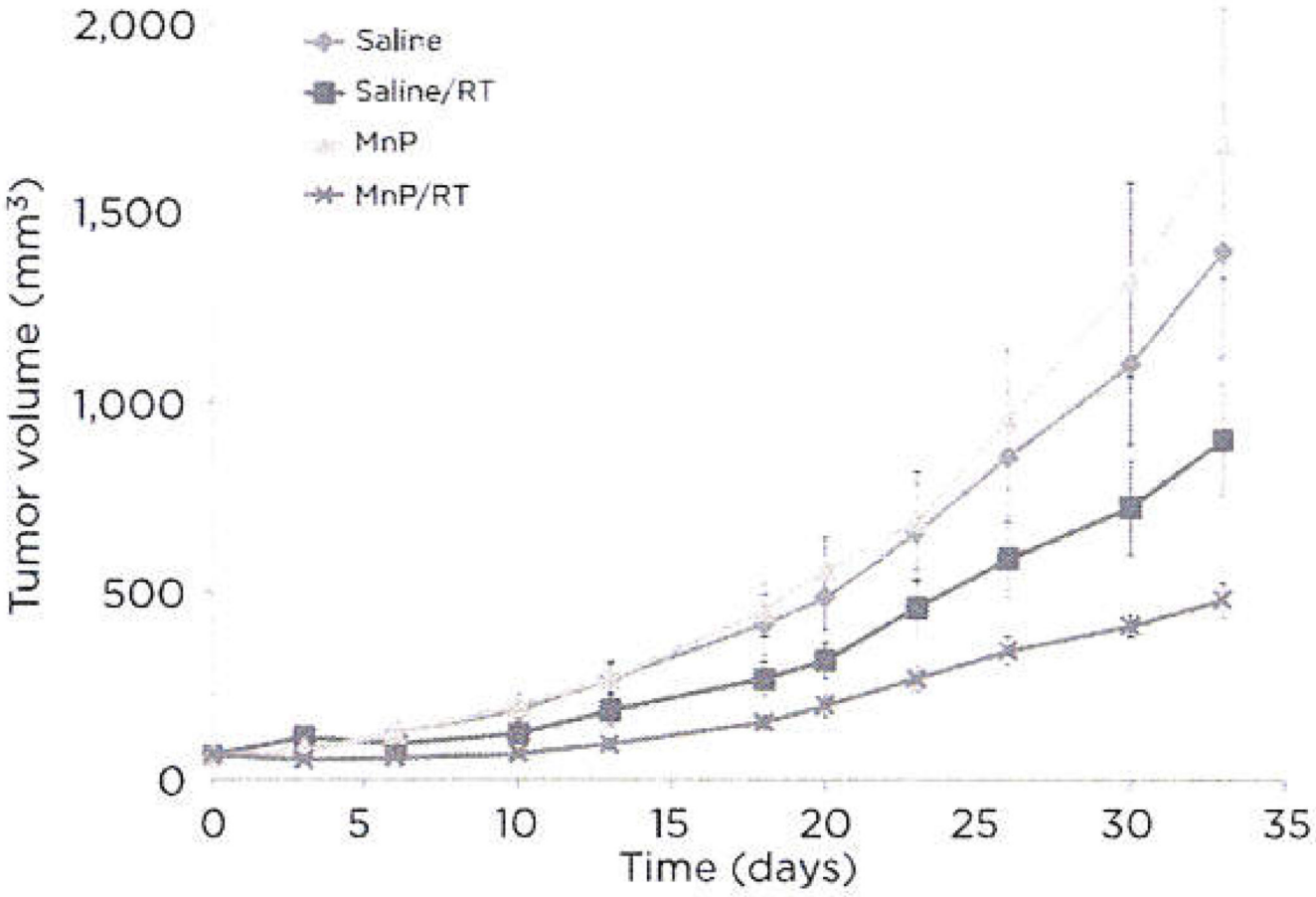

Figure 5.

Effects of MnTnBuOE-2-PyP^{5+} on flank tumor growth. Flank tumor growth assays were performed with D-245 MG cells in BALB/c mice. Eight mice per group were injected twice daily with saline or 1.6 mg/kg MnTnBuOE-2-PyP^{5+} for the duration of the study. A fractionated radiation dose of 3 × 1 Gy was performed on day 2. Statistics are discussed in Results.

Table 1

MS/MS analysis of MnP in mouse tissues (n = 2)

	Brain (nmol/L)	Liver (nmol/L)
MnP	31.30 ± 4.41	5,520 ± 872
MnP/RT	23.76 ± 1.32	4,935 ± 1,218